2022

Examining Ecological Succession of Diatoms in California Current System Cyclonic Mesoscale Eddies

Zuzanna M. Abdala
Old Dominion University, zabda001@odu.edu

Sophie Clayton
Old Dominion University, sclayton@odu.edu

Sveinn V. Einarsson
Old Dominion University

Kimberly Powell
Old Dominion University, kepowell@odu.edu

Claire P. Till

See next page for additional authors

Original Publication Citation

Abdala, Z. M., Clayton, S., Einarsson, S. V., Powell, K., Till, C. P., Coale, T. H., & Chappell, P. D. (2022). Examining ecological succession of diatoms in California Current System cyclonic mesoscale eddies. *Limnology & Oceanography*, *67*(11), 2586-2602. https://doi.org/10.1002/lno.12224

LIMNOLOGY and OCEANOGRAPHY

ASLO

Limnol. Oceanogr. 67, 2022, 2586–2602

doi: 10.1002/lno.12224

Examining ecological succession of diatoms in California Current System cyclonic mesoscale eddies

Zuzanna M. Abdala,[1] **Sophie Clayton**,[1] **Sveinn V. Einarsson**,[1] **Kimberly Powell**,[1] **Claire P. Till**,[2] **Tyler H. Coale**,[3] **P. Dreux Chappell**[1*]

[1]Department of Ocean and Earth Sciences, Old Dominion University, Norfolk, Virginia
[2]Department of Chemistry, California State Polytechnic University, Humboldt, Arcata, California
[3]J. Craig Venter Institute, La Jolla, California

Abstract

The California Current System is a diatom-dominated region characterized by seasonal coastal upwelling and additional elevated mesoscale activity. Cyclonic mesoscale eddies in the region trap productive coastal waters with their planktonic communities and transport them offshore with limited interaction with surrounding waters, effectively acting as natural mesocosms, where phytoplankton populations undergo ecological succession as eddies age. This study examines diatom community composition within two mesoscale cyclonic eddies that formed in the same region of the California Current System 2 months apart and in the California Current waters surrounding them. The diatom communities were analyzed in the context of shifting environmental gradients and through a lens of community succession to expand our understanding of biophysical interactions in California Current System cyclonic eddies. Diatom communities within each eddy were different from non-eddy communities and varied in concert with salinity and dissolved iron (Fe) concentrations. The younger, nearshore eddy displayed higher macronutrient and dissolved Fe concentrations, had higher values for diatom Shannon diversity and evenness, and had nutrient ratios indicative of either eventual silicic acid (Si) or Fe limitation or possibly co-limitation. The older, offshore eddy displayed low macronutrient and dissolved Fe concentrations, was likely nitrate-limited, and had lower diatom Shannon diversity and evenness indices. Sequences from the genus *Rhizosolenia*, some of which form vertically migrating mats to bypass nitrate limitation, dominated in the older eddy. This is of potential significance as the prevalence of *Rhizosolenia* mats could impact estimates of carbon cycling and export in the wider California coastal area.

As a region with elevated mesoscale activity, including extensive seasonal coastal upwelling resulting in frequent delivery of nutrients to the surface ocean, the California Current System is one of the most biologically productive regions in the world (Capone and Hutchins 2013). In many areas of the California Current System, silicic acid (Si) concentrations far exceed dissolved nitrogen (nitrate + nitrite, N) concentrations, allowing for a diatom-dominated phytoplankton community (Hood et al. 1990; Venrick 2009). Diatoms are unicellular eukaryotes that contribute ~ 25% of the global primary production, and ~ 40% of the primary production in the oceans (Round et al. 1990; Sumper and Brunner 2006). Because of their cellular structure, diatoms have an obligate Si requirement and are known to dominate phytoplankton communities in waters with elevated Si:N ratios, where they are important contributors to primary production and carbon (C) export (Sommer 1994; Dugdale et al. 1995; Smetacek 1999). Diatoms are the most abundant and diverse of eukaryotic marine phytoplankton groups, and their productivity is believed to significantly control fixed C availability for other trophic levels (Falkowski et al. 1998; Kooistra et al. 2007; Lewitus et al. 2018). The flux of organic C from sinking diatom blooms fuels the "biological C pump" that exports atmospheric C to the ocean interior (Smetacek 1999). Nutrient-rich coastal waters in the California Current System are home to elevated proportions of large diatoms (Hood et al. 1990).

*Correspondence: pdchappe@odu.edu

Additional Supporting Information may be found in the online version of this article.

Author Contributions Statement: C.P.T., P.D.C. and S.C. designed the underway sampling plan while P.D.C. and Z.M.A. conceived of the diatom community analysis plan. All authors contributed to sample processing and analysis of data. Z.M.A. and P.D.C. wrote the initial draft of the manuscript though all authors contributed substantially to editing of the manuscript and have approved the final submitted manuscript.

Nearshore dynamics, including coastal upwelling, mixing from opposing currents, and river outflows, have been shown to impact diatom community composition (e.g., Du and Peterson 2013). As diatom community composition is known to influence the magnitude of C export by varying Si:C ratios, cell size, and morphology (Treguer et al. 2018 and references therein), it is important to understand how diatom communities respond to environmental forcing.

The California Current System is characterized by a collection of currents, up/downwelling, and mesoscale activity typical of eastern boundary upwelling systems (Kurian et al. 2011; Combes et al. 2013). Upwelling events in such systems are known to be especially productive (Cushing 1971; Iles et al. 2012). Because of the elevated frequency of nutrient delivery due to these upwelling events, eastern boundary upwelling systems can support both larger abundances of phytoplankton biomass (blooms) and larger phytoplankton cells than other regions of the ocean, and reportedly support 50% of global fish production (Hood et al. 1990). This is in contrast to open ocean regions, which have lower frequencies of nutrient delivery, are commonly in a nutrient-limited state, and generally support lower phytoplankton biomass and cell sizes (Bibby et al. 2008; Brown et al. 2008). Vertical transport of nutrients into the euphotic zone occurs via two primary mechanisms—shoaling of isopycnals and coastal upwelling (Owen 1980; Biller and Bruland 2014). Seasonal shifts in wind direction control the presence and absence of upwelling, impacting nutrient distributions at the surface. In the summer, winds blow equatorward, leading to Ekman transport offshore and coastal upwelling; contrastingly, in the winter, prevailing winds switch to a poleward direction, causing Ekman transport onshore and downwelling along the coast (Du and Peterson 2013). Coastal upwelling in response to equatorward winds in the summer delivers waters with N, Si, and phosphate concentrations that range from 15–35, 15–45, and 1.3–2.6 μmol L^{-1}, respectively, which stimulate Chlorophyll *a* (Chl *a*) values between 10 and 35 μg L^{-1} at the surface (Bruland et al. 2001). These wind-driven upwelling events in the California Current System are typically dominated, at least initially, by diatoms, which are especially suited to respond to nutrient delivery associated with high turbulence (Benoiston et al. 2017). In addition, some diatoms in upwelling environments also appear to "frontload" the expression of genes related to N uptake, which is likely also a factor that influences their ability to outcompete other phytoplankton (Lampe et al. 2018). Following nutrient drawdown post upwelling, phytoplankton community succession in the California Current System can progress to a non-diatom dominated community (Wilkerson et al. 2006; Krause et al. 2020).

In addition to upwelling and downwelling, the California Current System is also subject to other vigorous mesoscale and submesoscale activity, with eddies and filaments playing a significant role in the movement of water and creating many sharp salinity and nutrient fronts (Nagai et al. 2015; Chenillat et al. 2016). Eddy formation occurs from baroclinic instability (Bibby et al. 2008; Kurian et al. 2011), which can result from many different factors, including coastline irregularities, upwelling filaments, seafloor topography, wind forcing, shearing from opposing currents, or a combination of these (Batteen et al. 2003). The complex bathymetry attributed to a triple junction results in elevated eddy kinetic energy and a high frequency of filament and eddy formation near Cape Mendocino (Nagai et al. 2015; Hoover and Tréhu 2017). California Current System eddies are highly nonlinear compared to eddies globally, meaning that their rotational speed is much faster than their speed of propagation, severely limiting exchange with surrounding waters (Kurian et al. 2011; Chenillat et al. 2018). California Current System eddies are highly efficient in trapping parcels of coastal water and transporting them offshore (Combes et al. 2013; Chenillat et al. 2016). These eddy-trapped water parcels often contain upwelled waters high in nutrient concentrations, and diatom communities with elevated diversity (Venrick 2009; Kurian et al. 2011). Upwelled nutrients are also advected offshore via filaments—responsible for most of the nutrient transport up to 100 km offshore—and surface and subsurface eddies—responsible for transport up to 200–800 km offshore (Combes et al. 2013; Nagai et al. 2015). In fact, 50% of the total transport of N in the California Current System has been attributed to mesoscale eddies (Chenillat et al. 2016, 2018). Because of this, mesoscale cyclonic eddies have been shown to support elevated productivity that is close to coastal levels for extended periods up to 1 year and up to 800 km offshore, increased phytoplankton photosynthetic efficiency, and play a substantial role in controlling the C cycling and export (Bibby et al. 2008; Brown et al. 2008; Chenillat et al. 2016).

An appreciation of the various physical influences on phytoplankton growth that eddies can impart, including how vertical movement changes light and nutrient availability and how those movements may change throughout an eddy's duration, has been known for some time (Flierl and McGillicuddy 2002 and references therein). More recent advances such as the ability to run eddy resolving models with multiple phytoplankton species (Clayton et al. 2013), have highlighted the need to gain a better understanding of how eddies influence phytoplankton diversity and community composition (McGillicuddy 2016 and references therein), yet there remains limited information regarding ecological succession of phytoplankton communities in eddies particularly in the California Current System. As regional differences in eddy dynamics have been well established (McGillicuddy 2016 and references therein), it is critical to perform regionally specific studies of how eddies influence phytoplankton communities. In the California Current System, the entrapment of coastal waters, combined with longer lifespans of cyclonic eddies, allows for coastal diatom communities within cyclones to undergo ecological succession as the eddies age and travel offshore (Owen 1980; Kurian et al. 2011). Coastal diatoms are

known to have higher macro- and micronutrient requirements than oceanic species, making them more susceptible to nutrient limitation and more likely to draw nutrients down rapidly (Marchetti et al. 2006). Thus, ecological succession within an aging eddy may result in a community adapted to the niche created by nutrient drawdown. There is some evidence to support this in a previous spatial study in the California Current System, which found diatom communities of similar composition in concentric circles around the center of an eddy, with each circle in a different stage of succession (Owen 1980). A temporal study of a cyclonic eddy near Hawaii also found that after the nutrients in the surface mixed layer had been depleted, the larger-celled, coastal diatoms were succeeded by smaller-celled, open ocean diatoms (Brown et al. 2008). Because of the wide spatial and temporal variability in community structures within eddies, there is a need to better understand the processes that drive community shifts within them as they propagate (Brown et al. 2008).

The combination of high frequency mesoscale activity, strong seasonality, and an extensive presence of diatoms makes the California Current System an ideal region to examine how eddy dynamics impact diatom communities. In this study, we examine a suite of ecological factors in two cyclonic California Current System eddies—an inshore eddy that was 22 d old at time of sampling having formed in mid-June and an offshore eddy that was 80 d old having formed in mid-April, both of which formed near Cape Mendocino. Our study combines measurements of hydrographic parameters, macro- and micronutrient concentrations, and an examination of diatom community composition using a high-throughput sequencing technique targeting diatoms (Chappell et al. 2019). The main hypotheses tested were: (1) diatom communities in the eddies are distinct from those of non-eddy surrounding waters; and (2) diatom community composition shifts associated with the two eddies of different ages correlate with changing physicochemical variables such as salinity and nutrient concentrations. We also include a discussion of our results in the context of ecological succession under the assumption that examining the diatom community composition of two eddies that originated from the same region 2 months apart can serve as a proxy for an in situ study of ecological succession of diatoms within a single California Current System eddy.

Methods

Environmental data

Sampling occurred 13–14 July 2014 on R/V Melville cruise MV1405 (Fig. 1). The cruise track began 430 km from the coastline of Northern California, traveled northeast, and pivoted midway to allow for sampling through the centers of two cyclonic eddies. This synoptic survey took 26 h, making it as close to a snapshot of the system as possible. Sea surface temperature (SST) and salinity were measured using an SBE 21 Thermosalinograph (SeaBird Electronics) and Chl *a* fluorescence was measured using a Turner 10 AU fluorometer from the flowthrough intake, the values of which were calibrated via chemical extraction of Chl *a* on board at the start of the cruise (data not shown). Wind speed was measured using a WindmasterPro Anemometer (Gill Instruments). Salinity, SST, Chl a, and wind speed data were smoothed into half-kilometer bins using the interp function of the NumPy toolkit (Harris et al. 2020) in Python (version 3.7.6). Potential density (σ_θ) was calculated using the Python implementation of the Gibbs SeaWater Oceanographic Toolbox of TEOS-10 (McDougall and Barker 2011).

In order to identify the location of the mesoscale eddies, we used 1/4° × 1/4° gridded daily sea level anomaly products that merge data from multiple satellites to obtain a high-resolution view of the dynamics of the upper ocean (the Ssalto/Duacs altimeter products produced and distributed by the Copernicus Marine and Environment Monitoring Service, CMEMS). In addition, we used the AVISO Mesoscale Eddy Trajectories Atlas (META 2.0) in order to track the trajectory of the eddies, and determine the time and location where they were initially formed.

Sample collection

A trace metal clean surface tow-fish system (Bruland et al. 2005) was used to collect water from 3–5 m depth at roughly 1-h intervals (n = 20 samples total) while the ship was underway (traveling at ~ 10 knots). One to two liters of water were filtered for DNA analysis onto 25-mm diameter, 3 μm polyester filters using a Masterflex peristaltic pump. Filters were placed in 2 mL screw-cap tubes with 400 μL of Qiagen RLT Plus Buffer (Qiagen), frozen in liquid N_2, and stored at −80°C until extraction. Concurrent water samples for macronutrient, dissolved iron (Fe), and dissolved manganese (Mn) analyses were filtered through an acid-cleaned, seawater-flushed 0.2 μm Acropak filter capsule (Pall 500; Fisher Scientific). Nitrate + nitrite (N), phosphate, and Si were analyzed onboard using a Lachat QuickChem 8000 Flow Injection Analysis System following standard spectrophotometric methods (Parsons 1984). Surface dissolved Fe and dissolved Mn were pre-concentrated and analyzed as in Biller and Bruland (2012) with the adaptations in Parker et al. (2016). Briefly, seawater samples were acidified at sea to pH ~ 1.7 using quartz-distilled HCl and stored in acid cleaned LDPE bottles for at least 2 months. Prior to analysis, acidified seawater was buffered to pH 6 and dissolved Fe and dissolved Mn were preconcentrated onto Nobias-chelate PA1 resin and then eluted off the column using quartz-distilled HNO_3. The eluent was then analyzed using a Thermo-Element high resolution XR ICP-MS, which was run in counting mode. One third of samples were analyzed in duplicate to assess precision. Based on replicate values of the particular samples reported in this work, the precision for Mn was 0.16 ± 0.10 nmol kg^{-1}, and the precision for Fe was 0.07 ± 0.07 nmol kg^{-1}. Accuracy was also assessed by

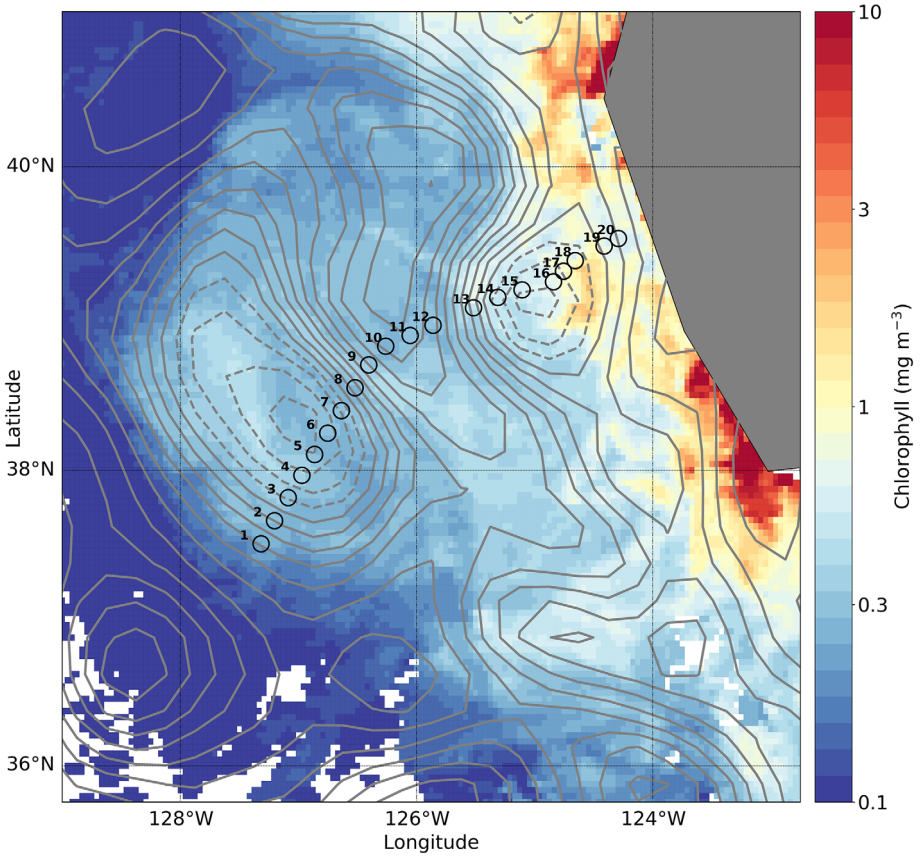

Fig. 1. Geographical location of the study site. Gray contours show sea level anomaly differences of 25 cm ranging from +2.5 m to −1 m from the Aviso dataset for satellite altimetry data for 13 July 2014, with negative sea level anomalies as dashed contours and positive sea level anomalies as solid contours. Stations are numbered in succession, beginning with Sta. 1 at the most-western point to Sta. 20 at the most-eastern point. Background color shows the monthly composite of Chlorophyll *a* for July 2014 from the MODIS instrument.

analyzing SAFe S and D2 reference samples. Over several ICPMS runs with this method, our lab obtained values for Mn of 0.81 ± 0.07 and 0.37 ± 0.04 nmol kg^{-1}, compared with consensus values of 0.79 ± 0.06 and 0.35 ± 0.05 nmol kg^{-1}. For Fe, our lab obtained 0.095 ± 0.014 and 0.94 ± 0.17 nmol kg^{-1}, compared with consensus values of 0.093 ± 0.008 and 0.93 ± 0.02 nmol kg^{-1} (SAFe May 2013 Consensus values). Calculations of Fe:N and Si:N were performed to identify the potential for nutrient limitation at the sampled stations with Fe:N of 0.2 and 0.07 nmol:μmol used to define the Fe vs. N limitation cutoff for coastal and open ocean diatoms, respectively, and Si:N of 1 used as the Si vs. N limitation cutoff (Levasseur and Therriault 1987; Biller and Bruland 2014). The potential for deficiency of dissolved Mn relative to dissolved Fe for phytoplankton growth (Mn*) was calculated following the equation in Browning et al. (2021) such that Mn* = Mn − (Fe/2.67).

DNA extraction and amplicon sequencing and processing

DNA was extracted from filters using the Qiagen Allprep RNA/DNA co-extraction with an additional bead-beating step and homogenization using the QIAshredder column (Qiagen). The V4 region of the 18S rDNA was amplified and sequenced using the general procedure described in Chappell et al. (2019) with modifications described in Oliver et al. (2021). Briefly, the diatom 18S rDNA V4 region was amplified from each sample in triplicate using polymerase chain reaction and diatom specific primers (Chappell et al. 2019), triplicates were gel purified and pooled and then samples were multiplexed using a Nextera DNA Library Preparation Kit (Illumina) and sequenced on the Illumina MiSeq platform (Illumina) using the Illumina v3 2 × 300 cycle kit. Diatom 18S rDNA amplicon sequences were de-multiplexed and analyzed using the DADA2 pipeline (version 1.16.0; Callahan et al. 2016) with modifications described in Oliver et al. (2021), which produces amplicon sequence variants (ASVs). Taxonomic assignment of the ASVs followed the protocol of Chappell et al. (2019) using a nucleotide BLAST (Altschul et al. 1990) against an in-house database that combined Stramenopile 18S sequences from NCBI (downloaded as of 23 June 2020) and the SILVA 18S database. Only ASVs with a diatom top hit were included in subsequent analyses. ASVs were classified to the species level if they had a > 99% identity to a diatom sequence, as species-like (akin to the cf. designation) if they had 98–99% identity, and classified to the genus level when identity was < 98%. As

classifying down to ASVs may look at intraspecies variability rather than interspecies variability (Caron and Hu 2019), ASV clustering into operational taxonomic units (OTU_{99}) was performed using the CD-HIT algorithm (Li and Godzik 2006) if they had < 1% percent identity difference. Raw sequence data has been submitted to NCBI SRA under the BioProject Accession PRJNA743307.

Community composition analyses

Analysis of alpha diversity indices, specifically the calculation of species richness (S) and Shannon entropy (H') was performed on both ASV and OTU_{99} count data in R version 4.1.1 (Shannon 1948; R Core Team 2021) using packages designed to account for the compositional nature of high-throughput amplicon sequencing datasets (Gloor et al. 2017), specifically "Breakaway" and "DivNet" (Willis and Bunge 2015; Willis and Martin 2022), which provide standard error/variance estimates. These values were then used to calculate Pielou's evenness (J') (Pielou 1966) using the eq. $J' = H'/\ln(S)$. Shannon entropy (H') was converted to the exponential Shannon diversity index (^1D) using the equation $^1D = \exp(H')$ (Jost 2006). Analysis of beta diversity, specifically the calculation of Bray–Curtis dissimilarity (Bray and Curtis 1957), was only performed on OTU_{99} count data and was calculated using "DivNet" (Willis and Martin 2022) for compositional data. Bray–Curtis was chosen over a presence-absence statistic specifically because of concerns with sequencing depth variation between samples that is also associated with high throughput sequencing data (Gloor et al. 2017 and references therein). Diatom and dinoflagellate 18S copy number per cell is known to vary in relation to biovolume (Godhe et al. 2008). As attempting to scale our analyses using estimates of each diatom species' biovolume would likely introduce more error into our analyses, we present these data as is.

Statistical analyses

Kruskal–Wallis tests were conducted comparing variables at molecular sampling locations among three groups: eddy I, eddy II, and non-eddy (Kruskal and Wallis 1952). Kruskal–Wallis test was chosen because the number of sampling points in each group was uneven and variables either had a non-normal distribution or the residuals from ANOVA were non-normally distributed. Dunn's post hoc tests were then performed to obtain detailed differences between each set of groups: eddy I vs. eddy II, eddy I vs. non-eddy, and eddy II vs. non-eddy (Dunn 1964).

To determine the single environmental factor or group of environmental factors that best explained the dissimilarity distribution of these data, scaled environmental data and the OTU_{99} Bray–Curtis dissimilarity matrix were analyzed using the BIOENV algorithm in the R package "vegan" using the Spearman rank correlation method and 1000 permutations (Clarke and Ainsworth 1993; Oksanen et al. 2020). Environmental factor multivariate statistical analyses could only be performed on the subset of stations where all factors were measured, thus Stas. 1, 13, and 18 were omitted from the BIOENV and subsequent factor-associated statistical analyses. The statistical significance of the BIOENV results were subsequently assessed by performing Mantel tests using the factor(s) highlighted in BIOENV results (Mantel 1967). Following BIOENV/Mantel analysis, permutational multivariate ANOVA (PERMANOVA) tests were performed to confirm whether Bray-Curtis distances significantly correlated with the environmental factors identified in BIOENV analyses using the adonis2 function and 1000 permutations in the R package "vegan" (Oksanen et al. 2020). As PERMANOVA is an alternative non-parametric multivariate statistical test that can also evaluate differences based on categorical groupings, a separate PERMANOVA analysis was performed using the full diatom community dataset to test whether eddy station classifications correlated significantly with Bray-Curtis distances. Finally, canonical analysis of principal coordinates analysis was performed using the Bray–Curtis distances and

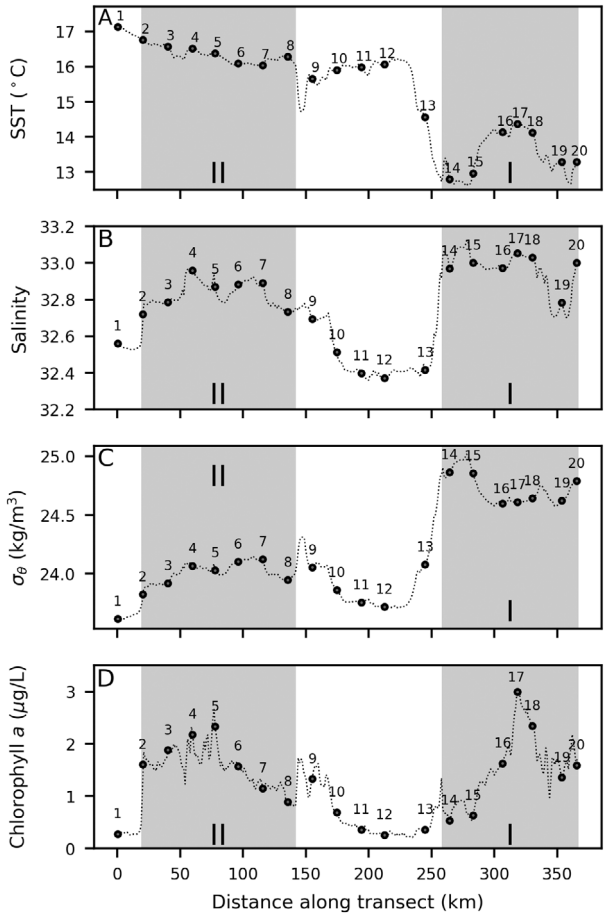

Fig. 2. Underway measurements of sea surface (**a**) temperature (SST), (**b**) salinity, (**c**) potential density (σ_θ), and (**d**) Chlorophyll *a*. Numbers above the circles are the station numbers for discrete sample collection. Gray boxes represent the boundaries of eddies I and II.

the subset of environmental factors that significantly correlated with them by BIOENV/Mantel/PERMANOVA analysis using the "CAP" method in the ordinate function of the "Phyloseq" R package (Anderson and Willis 2003; McMurdie and Holmes 2013).

Results

Environmental data

Sampling locations are shown superimposed on gridded sea level anomaly for July 13, 2014 over a monthly composite of Chl *a* for July 2014 (Fig. 1). The highest values for satellite chl *a* were found along the coast (10 mg m^{-3}) and lowest values were offshore (0.1 mg m^{-3}). Based on a combination of closed contours of sea level anomaly centered around a negative sea level anomaly and in situ water mass characteristics (SST, salinity, and σ_θ), we defined the boundaries of the eddies. From this point on, Stas. 14–20 (nearshore) will be referred to as "eddy I" and Stas. 2–8 (offshore) will be referred to as "eddy II." The negative sea level anomaly was −1 m at the center of eddy II and −0.75 m at the center of eddy I. The positive sea level anomaly was 1.75 m in the center of the transect between the two eddies. The age, track, and diameter of the individual eddies was determined using the Aviso Mesoscale Eddy Trajectory Atlas (SSALTO/DUACS n.d.), which is based on remotely sensed sea surface height data. Eddy I was first identified on 18 June 2014 at 124.9°W 39.5°N, 22 d before it was sampled, and eddy II was first identified on 21 April 2014 at 125.5°W 39.2°N, 80 d before it was sampled. The eddies were formed within 50 km and 58 d of each other, with eddy II traveling offshore and eddy I remaining closer to the coast (the eddy tracks are shown in Fig. S1). At the time of sampling, eddy I had a diameter of 116 km and eddy II had a diameter of 212 km.

Elevated salinity data from both eddies indicates that deeper waters had upwelled to the surface at some time in the past (Fig. 2). Environmental parameters are reported as averages ± standard deviation by region throughout the manuscript. The average SST in eddy I was 13.5 ± 0.6°C, whereas the average SST in eddy II and the non-eddy region were similar (16.3 ± 0.2°C and 16.3 ± 0.4°C, respectively; Fig. 2a). This lower SST in eddy I combined with the wind speed data (Fig. S3A) suggests that parts of eddy I may still have been experiencing upwelling at the time of sampling. Surface salinity was elevated in eddies I and II (32.96 ± 0.11 and 32.83 ± 0.08, respectively) compared to non-eddy regions (32.44 ± 0.07, Fig. 2b). Surface σ_θ values ranged from 23.48 to 24.90 kg m^{-3} (Fig. 2c) with higher values in eddy I (24.59 ± 0.13 kg m^{-3}) and lower values in both eddy II and the non-eddy region (23.90 ± 0.08 and 23.61 ± 0.07 kg m^{-3}, respectively). As SST, salinity, and σ_θ differences were used to define eddy boundaries, statistics are not reported for those parameters. Chl *a* ranged from 0.21 to 3.06 μg L^{-1} (Fig. 2d) and was found to be significantly different across the three regions with post hoc tests revealing that elevated fluorescence in eddies I and II (1.15 ± 0.63 and 1.15 ± 0.63 μg L^{-1}, respectively) were significantly different from fluorescence at the non-eddy stations (0.37 ± 0.16 μg L^{-1}) but not from one another (Table 1).

Macronutrient concentrations including N (Fig. 3a), phosphate (Fig. 3b), and Si (Fig. 3c) were significantly higher in eddy I (5.18 ± 1.93, 0.62 ± 0.12, and 3.11 ± 0.78 μmol kg^{-1}, respectively) compared to those measured in either eddy II (0.91 ± 0.84, 0.33 ± 0.03, and 1.73 ± 0.53 μmol kg^{-1}, respectively) or the non-eddy region (0.28 ± 0.30, 0.31 ± 0.02, and 1.55 ± 0.33 μmol kg^{-1}, respectively) with nutrient concentrations in the latter two regions not being statistically different from one another (Table 1). Si:N ratios were generally below one in eddy I, slightly above one in eddy II, and well above

Table 1. Kruskal–Wallis (KW) test results for groups defined as eddy I, eddy II, non-eddy and results of Dunn's post hoc test to determine which groups are significantly different.

Factor	KW: Between groups df	KW: # of observations	KW *H* statistic	KW *p* value	Dunn's eddy I vs. eddy II	Dunn's eddy I vs. non-eddy	Dunn's eddy II vs. non-eddy
Fluorescence	2	18	7.7	$p<0.05$*	$p=1$ NS	$p=0.05$*	$p<0.05$*
N	2	18	14.5	$p<0.001$*	$p<0.05$*	$p<0.01$*	$p=0.38$ NS
Si	2	18	12.2	$p<0.01$*	$p<0.01$*	$p<0.05$*	$p=1$ NS
Phosphate	2	18	13.3	$p<0.005$*	$p<0.05$*	$p<0.005$*	$p=1$ NS
Fe	2	16	10.7	$p<0.005$*	$p<0.005$*	$p=1$ NS	$p=0.14$ NS
Mn	2	17	7.9	$p<0.05$*	$p=1$ NS	$p<0.05$*	$p=0.12$ NS
Rhizosolenia_6	2	18	12.2	$p<0.01$*	$p<0.01$*	$p=1$ NS	$p<0.05$*
OTU ^{1}D	2	18	14	$p<0.001$*	$p<0.05$*	$p=0.34$ NS	$p<0.001$*
OTU *J′*	2	18	14.9	$p<0.001$*	$p<0.05$*	$p=0.30$ NS	$p<0.001$*
ASV ^{1}D	2	18	14.5	$p<0.001$*	$p<0.05$*	$p=0.38$ NS	$p<0.005$*
ASV *J′*	2	18	14.5	$p<0.001$*	$p<0.05$*	$p=0.38$ NS	$p<0.001$*

*Significant results.

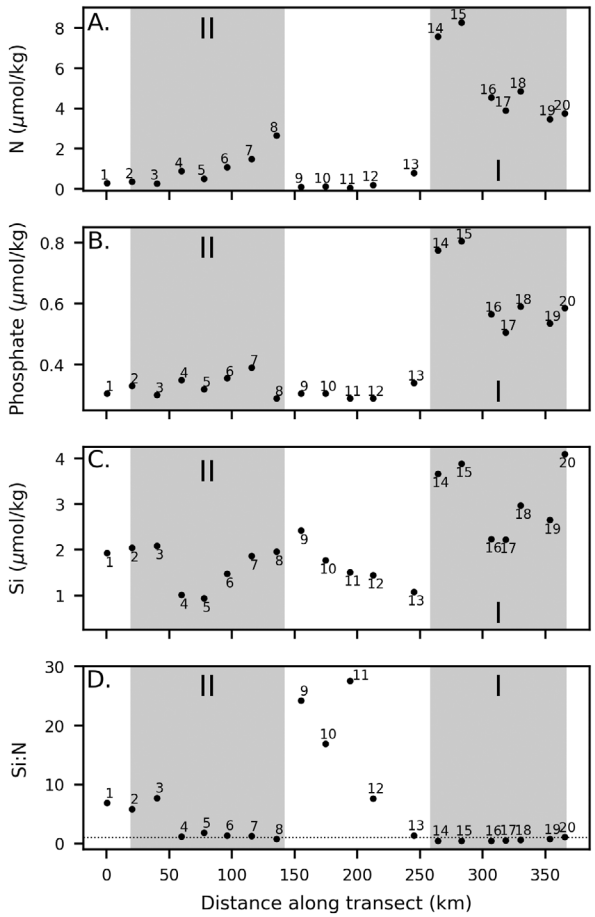

Fig. 3. Measurements of surface macronutrient concentrations along the cruise track (**a**) N, (**b**) Si, (**c**) phosphate, and (**d**) calculated Si:N ratio with dotted line placed at a value of 1. Numbers above the datapoints and gray boxes as described in Fig. 2.

one in non-eddy regions (Fig. 3d). Dissolved Fe concentrations (Fig. 4a) were significantly different between the three regions with post-hoc analysis revealing that the only truly significant differences in dissolved Fe concentrations were between eddy I, which had the highest dissolved Fe concentrations (0.41 ± 0.07 nmol kg^{-1}), and eddy II (0.11 ± 0.08 nmol kg^{-1}), which had the lowest dissolved Fe concentrations (Table 1). Values in the three non-eddy stations with dissolved Fe data showed high variability (0.21 ± 0.17 nmol kg^{-1}). Dissolved Mn concentrations were highest at the non-eddy stations (2.78 ± 0.39 nmol kg^{-1}) and lower at stations in both eddy I and eddy II (1.92 ± 0.13 and 1.98 ± 0.16 nmol kg^{-1}, respectively; Fig. 4b). Overall, dissolved Mn concentrations were significantly different between groups, but post hoc analysis revealed that only the differences between eddy I and the non-eddy region were significant (Table 1). Mn* was significantly above zero for the entire transect (Fig. 4c). Dissolved Fe:N ratios were below 0.2 nmol:μmol in both eddies and above 0.2 nmol:μmol in non-eddy regions (Fig. 4d).

Alpha diversity measures

Alpha diversity analysis on both ASV and OTU_{99} data confirmed that overall trends were similar and that condensing to OTU_{99} did not mask any important differences in diatom sequence distributions between stations or regions (Figs. 5 and S2A; Tables S1 and S2). Species richness, which is a measure of the number of ASVs/OTU_{99} in each sample, showed no specific trends by region though, not surprisingly, richness values were higher when ASV data were used in analysis (Fig. S2A) than when OTU_{99} data were used (Fig. 5a). Exponential Shannon diversity (Figs. 5b and S2B), which is a diversity metric that combines information on species richness and how much the relative abundance of individual species diverge from being equally represented, and Pielou's evenness (Figs. 5c and S2C), which is an estimation of how equal the representation of individual species is in a sample, were both significantly lower in eddy II than in eddy I or the non-eddy regions regardless of whether OTU_{99} or ASV data were used in analysis (Table 1). This drop in Exponential Shannon diversity and evenness was likely driven by the changing relative abundance of an OTU_{99} from the genus *Rhizosolenia* (Fig. 5d; Table S2), which increased significantly in relative abundance in eddy II compared to eddy I and non-eddy regions (Table 1).

Diatom community composition and multivariate analyses

The non-metric multidimensional scaling (NMDS) plot of Bray–Curtis dissimilarity (Fig. 6a) shows that samples from each of the two eddies and the non-eddy regions clustered together. PERMANOVA analysis found that eddy classification (eddy I, eddy II, non-eddy) explained 59% of the variability observed in the Bray–Curtis distance matrix ($p < 0.01$). Subsequent PERMANOVA analyses comparing Bray–Curtis distances between stations associated with each region (essentially a post hoc analysis) revealed that all differences were significant (all adjusted $p < 0.01$). Multivariate statistical analyses performed on the subset of stations where all environmental factors were measured were used to explore how variations in environmental factors correlated with diatom community shifts, in other words, how the physicochemical properties of the different regions could potentially be driving these community differences. While there were some differences in the R^2 values based on the different tests, which are generally interpreted as representing the percentage of the Bray–Curtis distance that can be explained by a factor or group of factors based on each test, the overall patterns in the multivariate analyses were the same (Table 2). The single environmental factor that explained the most variability in the diatom community regardless of the statistical test used was dissolved Fe and the "pair" of factors that combined could explain 68% of the variability was dissolved Fe and salinity. Other factor pairs that produced significant correlations were dissolved Fe and dissolved Mn, dissolved Fe and SST, and SST and salinity. The canonical analysis of principal coordinates analysis found that

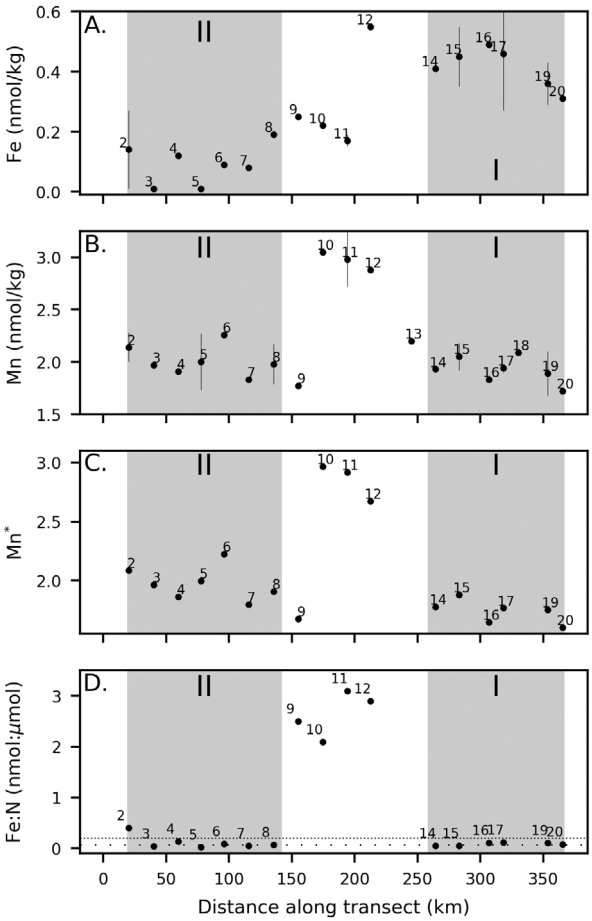

Fig. 4. Measurements of trace metal micronutrient concentrations along the cruise track (**a**) dissolved Fe, (**b**) dissolved Mn, (**c**) calculated Mn*, and (**d**) calculated Fe:N ratio (datapoints) with tightly dotted line placed at Fe:N value of 0.2 nmol:μmol and loosely dotted line placed at Fe:N value of 0.07 nmol:μmol. Numbers above the datapoints and gray boxes as described in Fig. 2. Error bars in (**a**) and (**b**) represent the standard deviation of duplicate measurements, which was only for seven of the stations.

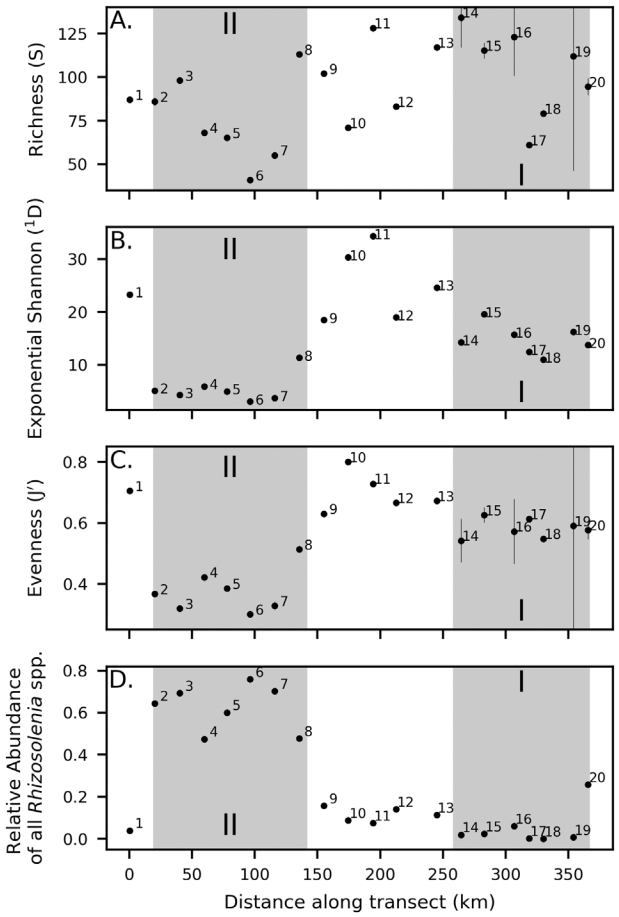

Fig. 5. Diversity indices based on OTU_{99} groupings. (**a**) Species richness, (**b**) Exponential Shannon diversity, (**c**) Pielou's evenness, (**d**) relative abundance of the *Rhizosolenia* genus. Numbers above the datapoints and gray boxes as described in Fig. 2. Error bars in (**a**) represent $\pm$ 2 standard errors in species richness as estimated by "Breakaway." Error bars in (**b**) and (**c**) are based on error propagation of the richness and Shannon entropy errors (from "DivNet") as used to calculate evenness and exponential Shannon.

48% of variability in the Bray–Curtis distances could be explained by coordinate 1 (CAP1) with an additional 17% could be explained by coordinate 2 (CAP2; Fig. 6b). Overlaying the environmental variables on the plot shows that CAP1 is most closely associated with variations in dissolved Fe and SST with CAP2 being most closely associated with variations in salinity and dissolved Mn.

Only diatom genera that represented at least 10% of the sequencing reads in at least one sample are identified in the relative abundance columns (Fig. 6c). *Rhizosolenia* genus sequence reads clearly dominated in eddy II, while the composition of the core of eddy I was dominated by a mix of the genera *Actinocyclus* and *Fragilariopsis*. At the stations on the outer edges of eddy I, *Thalassiosira*, *Chaetoceros*, and *Asteromphalus* reads also became elevated in relative abundance. A table with all OTU_{99} and ASV identities and read counts are provided in the supplemental materials (Tables S1 and S2). The OTU_{99} with the highest read count, which dominated the reads from the eddy II stations, was most similar in sequence to that of *Rhizosolenia shrubsolei*, however, the sequence match between this OTU_{99} and *R. shrubsolei* was only 91% (Table S1). For this reason, this sequence is only classified to the genus level (*Rhizosolenia* sp. 6). The top five species in 18S gene abundance along the transect (based on read counts) were *Rhizosolenia* sp. 6, *Actinocyclus* sp. MPA-2013, *Thalassiosira diporocyclus*, *Asteromphalus* sp. TN-2014, and an OTU_{99} with > 98% similarity to *Fragilariopsis doliolus*.

Discussion

This study sampled two eddies that formed in roughly the same region (Cape Mendocino) ~ 2 months apart, allowing us

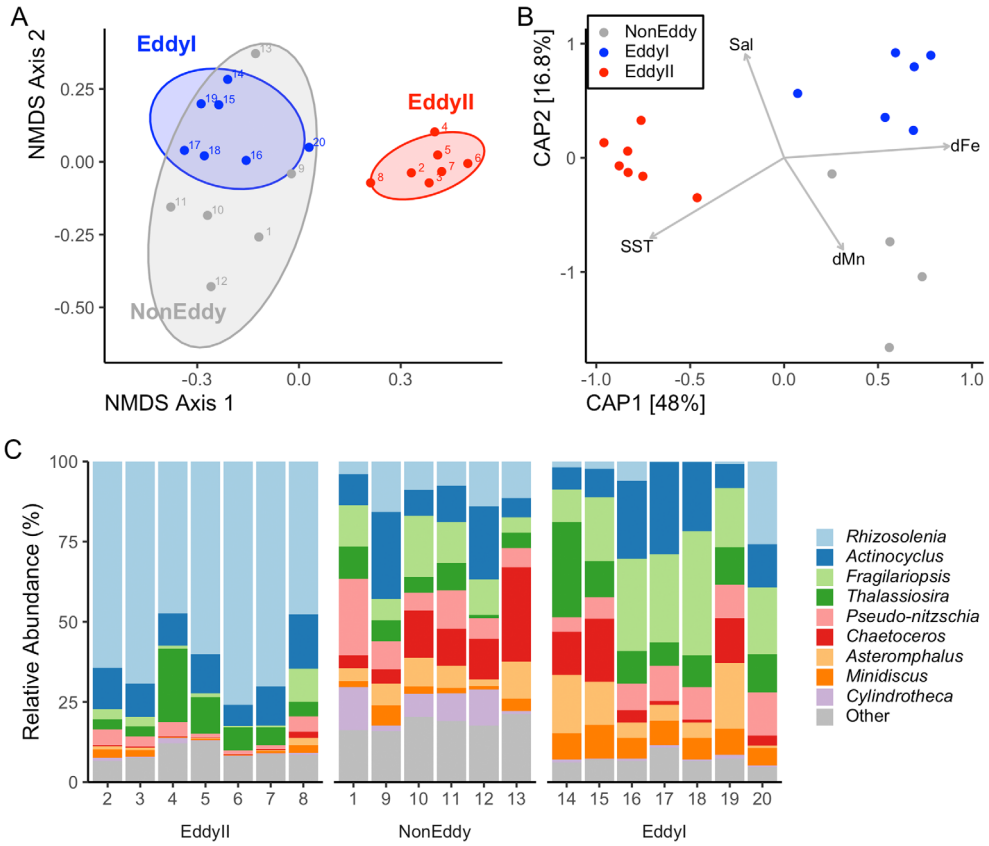

Fig. 6. Diatom community composition and multivariate analyses. (**a**) Non-metric multidimensional scaling (NMDS) plot of Bray–Curtis dissimilarity of diatom community composition based on OTU_{99} data for all stations. NMDS stress was 0.13. (**b**) Plot of the first two axes of the canonical analysis of principal coordinates (CAP) comparing Bray–Curtis dissimilarity of OTU_{99} for the subset of stations where all environmental factors were measured with the environmental factors used in the analysis plotted as directional vectors associated with the two axes plotted. Environmental factor abbreviations: Sal = salinity, dFe = dissolved Fe, dMn = dissolved Mn. Legend in b refers to the coloring of stations based on eddy grouping in both a and b. (**c**) Bar plot showing the relative abundance of reads associated with different diatom genera at each station with the stations grouped by eddy classification. Only diatom genera that accounted for at least 10% of the reads at a station are named. All other diatom genera reads are combined in the "other" category.

Table 2. Results from BIOENV/Mantel and PERMANOVA tests comparing variability in Bray-Curtis distance with variability in scaled environmental factors individually or assessed as pairs. PERMANOVA (add) "R" values is the sum of variability explained by the two factors without additional variability of any significant interaction. PERMANOVA (mult) "R" values add the interaction component if the interaction was significant.

Variable (s)	Mantel R	Mantel *p* value	PERMANOVA R (add)	PERMANOVA *p* value (add)	PERMANOVA R (mult)	PERMANOVA *p* value (mult)
Fe	0.59	$p<0.001$*	0.39	$p<0.001$*	NA	NA
Salinity	0.36	$p<0.005$*	0.17	$p<0.001$*	NA	NA
SST	0.34	$p<0.005$*	0.33	$p<0.001$*	NA	NA
Mn	0.22	$p<0.05$*	0.17	$p<0.005$*	NA	NA
Fe-Sal	0.68	$p<0.001$*	0.57	$p<0.005$*	0.69	$p<0.01$*
Fe-Mn	0.65	$p<0.001$*	0.56	$p<0.001$*	0.67	$p<0.01$*
Fe-SST	0.59	$p<0.001$*	0.55	$p<0.01$*	NA	$p=0.3$
Sal-SST	0.58	$p<0.001$*	0.61	$p<0.005$*	NA	$p=0.6$

NA, not applicable.
*Significant results.

to examine California Current System eddies through the lens of diatom community structure, geochemical measurements, and hydrography. Our analyses revealed strong differences among the three regions (eddies I, II, and non-eddy) in both physicochemical properties and diatom community composition that are consistent with an understanding of the nature of eddy formation and dynamics.

California Current System eddy structuration

The formation and development of cyclonic mesoscale eddies in the California Current System have been studied and modeled in depth (Chenillat et al. 2016, 2018). The outermost ring of an eddy is the youngest and latest addition and is composed of water from a variety of regions including recently upwelled waters (Chenillat et al. 2018), which creates a strong front on the western boundary of the eddy, especially in newly developed California Current System eddies. In examining the physicochemical measurements from eddy I, it is likely that newly upwelled waters had recently wrapped around eddy I at the time of sampling, resulting in the dramatic shifts in temperature, salinity, and nutrient concentrations crossing from California Current water (Sta. 13) into eddy I (Sta. 14). Chlorophyll measurements at Stas. 14 and 15 (sampled at 18:00 h and 19:00 h PST, respectively) were surprisingly low for their macronutrient concentrations. There are three possible hypotheses to explain the low observed chlorophyll fluorescence at these stations: (1) Non-photochemical quenching, a protective mechanism that photosynthetic organisms including diatoms use to protect photosystems from high light (Kiefer 1973), which has been shown to reduce fluorescence yields measured in ocean settings by 50% when PAR is $>1000\ \mu$mol quanta m^{-2} s^{-1} (Behrenfeld and Boss 2006); (2) Micronutrient limitation, such as low availability of dissolved Fe, which could explain why phytoplankton were not able to draw down macronutrients at these stations (Bruland et al. 2001); or (3) sampling occurred in a prebloom stage where nutrient drawdown had yet to occur (Engel et al. 2002). Because it was still daylight when these stations were sampled, it is possible that they were impacted by the non-photochemical quenching effect, however it seems unlikely that this is solely responsible for the low values as PAR values measured at Sta. 15 were low (~ 200) yet chlorophyll fluorescence was still reduced. Even with a 50% increase that might have occurred with PAR >1000 (Behrenfeld and Boss 2006) as it was at Sta. 14, chlorophyll fluorescence values would still be low at these stations. The second hypothesis can likely also be dismissed as dissolved Fe and dissolved Mn concentrations were elevated at these two stations, thus it seems unlikely that micronutrient limitation was limiting phytoplankton growth and macronutrient uptake. Based on this reasoning, we suggest that the third hypothesis, that we sampled a prebloom stage, is the most likely because the lowest SSTs and highest macronutrient concentrations in these samples suggest upwelling was recent if not ongoing at the time of sampling. In addition, the diatom communities at the two stations were distinct from the rest of eddy I. The NMDS plot showing Bray–Curtis dissimilarity for eddy I reflects that diatom community structure varies both with distance from the center of the eddy and the hydrographic structure of the eddy. Stas. 14 and 15 diatom communities group together, which is likely because this station includes recently upwelled waters indicated by low SST and elevated salinity as discussed above. The community from Sta. 19 is also grouped with Stas. 14 and 15, which may also indicate greater exposure to upwelling as it is in the outer ring of eddy I, though SST was not as low and salinity was not as high as at Stas. 14 and 15. Sta. 20, while also on the outer ring, has a diatom community composition that is separated from the rest of the eddy I stations, which may reflect additional interactions with the nearshore environment including access to additional runoff to the coast. Finally, the diatom communities from Stas. 16–18 grouped together, likely defining the originally trapped parcel of water and center of eddy I, having undergone a 22 d succession since formation. Indeed, the SST is elevated at these three stations compared to the other eddy I stations, suggesting upwelling did not occur recently. Previous work has suggested it takes up to 3 d of relaxation post upwelling for diatom communities to fully develop in response to California Current System upwelling events (Wilkerson et al. 2006; Closset et al. 2021). The elevated chlorophyll, reduced nutrient concentrations, and grouping of diatom communities at Stas. 16–18 could reflect a similar dynamic whereby an upwelling influenced community had been able to grow in at these stations.

Eddy II was 2 months older and had propagated further offshore than eddy I at the time of sampling leading to differences in both physicochemical and biological characteristics. Eddy II had higher SST than eddy I, which is not surprising considering that these surface waters had been exposed to extensive solar radiation since their last encounter with cold upwelled waters. The salinity measurements in eddy II resembled a tiered structure. Based on this structure, we defined Stas. 5 and 6 as the center of eddy II, with Stas. 4 and 7 as part of a circle around Stas. 5 and 6. The outer circle was composed of Stas. 2 and 3 on the western side of the eddy and Sta. 8 on the eastern side of the eddy. Overall, the diatom communities in the eddy II stations group together more tightly than those in eddy I. That said, diatom communities at some stations grouped closer together than others and these groupings did not always line up perfectly with the groupings of stations by salinity. We note that while salinity and σ_θ could support grouping Sta. 9 as part of eddy II, remotely sensed SLA does not place this station in a closed contour around a negative SLA anomaly. In addition, there was a significant drop in SST and a slight increase in salinity between Stas. 8 and 9 that may be a signature of localized, small-scale upwelling, which could also explain the increase in Chl *a* and N in the same region. For these reasons, Sta. 9 is not considered to be part of

eddy II. Indeed, Sta. 9 diatom community composition grouped most closely with the communities in eddy I. At the western boundary of eddy II, we saw dramatic changes in diatom community composition and decreases in both diatom diversity and evenness between Sta. 1, outside of eddy II, to Sta. 2, inside eddy II. The eddy II boundary between Stas. 1 and 2 was also associated with an increase in salinity and a significant increase in chlorophyll (noting that Sta. 1 was sampled at midnight). As for the non-eddy stations, there was less similarity of the diatom communities among the non-eddy stations compared to the community similarities seen within the eddies.

Nutrient ratios and multivariate analyses

Eddy I was high in both macro- and micro-nutrients, though nutrient ratios (Si:N < 1; Fe:N < 0.2 nmol:μmol) suggest the potential for these waters to progress towards Fe and/or Si limitation. The broad shelf area off Cape Mendocino has previously been described as an Fe-replete region (Bruland et al. 2001). However, the potential for Fe-limitation in a normally Fe-replete region was shown during the same cruise in a moderate shelf region off Cape Blanco, Oregon, just 300 km north (Till et al. 2019). It is also worth noting that while Si has not typically been thought to be a limiting nutrient for diatoms in the NE Pacific (Wilson and Qiu 2008), recent work, including analyses from this cruise, have found evidence of Si limitation in the California Current System (McNair et al. 2018; Closset et al. 2021). The Si:N ratios from eddy I suggest that eventual Si limitation was possible during macronutrient drawdown and that non-siliceous phytoplankton may also have been important contributors to the community, which our analyses would not capture. It has also been shown in some regions of the California Current System that diatoms experiencing Fe limitation can become more silicified by increasing their Si:N uptake ratios (Hutchins and Bruland 1998; Hutchins et al. 1998). This could lead to an eventual Fe and Si co-limitation scenario as eddy I waters age, though at the time of sampling macro- and micro-nutrient concentrations were still high in eddy I, so we do not think diatoms were currently growth limited by either Fe or Si.

Nutrient concentrations in eddy II were much lower than eddy I, which is not surprising given the likelihood that eddy II trapped a coastal phytoplankton community when it formed, and experienced limited exchange with non-eddy waters as it transited offshore. Thus, reduced access to nutrient-rich coastal waters and sustained photosynthetic activity by a nutrient-demanding coastal phytoplankton community would have led to the depletion of nutrients. Looking at Si:N ratios, eddy II had the potential to be limited by N (Si:N > 1) at all stations except Sta. 8. This shift in nutrient ratios from Si:N < 1 to Si:N > 1 between the two eddies would suggest preferential drawdown of N over Si, which would require the presence of a phytoplankton community that included non-diatoms, as the lowest Si:N drawdown observed in Fe replete waters has been found to be 1 (Brzezinski et al. 2002) or an elevated ratio of Si:N in the initial parcel of water that was trapped by the eddy when it formed. Assuming the eddy II diatom communities were coastal and had a Fe:N limitation threshold of 0.2 nmol:μmol (Biller and Bruland 2014), the Fe:N ratios of suggest that the surface waters in eddy II had the potential to be limited by N at Sta. 2 and limited by Fe at the remaining stations. If the diatom community had progressed to one that includes open ocean diatoms that have a Fe:N limitation ratio of 0.07 nmol:μmol (Biller and Bruland 2014), diatom communities in the surface waters at Stas. 4 and 6 may have also been N-limited. The potential role of Fe in shaping diatom community structure in the region is further supported by multivariate correlation analyses that found dissolved Fe to be among the environmental factors that, either alone or when combined with salinity or SST, had statistically significant correlations with diatom community composition.

We note that multivariate analyses also found dissolved Mn to correlate with changes in diatom community composition when combined with changes in dissolved Fe. Like Fe, Mn is a bioactive trace metal required in elevated quantities by phytoplankton for their photosynthetic machinery (Raven et al. 1999). Generally, surface drawdown of dissolved Mn is not as prevalent as has been observed for dissolved Fe (Morel et al. 2003) with an exception being the Southern Ocean, where dissolved Mn concentrations have been found to be exceedingly low (e.g., Martin et al. 1990; Middag et al. 2011, 2013). Lab culture experiments have found evidence that both temperate and Southern Ocean diatoms can experience dissolved Mn limitation of primary production (Sunda and Huntsman 1983, 1996; Pausch et al. 2019). It is only recently, however, that Fe–Mn co-limitation has been observed in the field and this has only been observed in incubation experiments with Southern Ocean phytoplankton communities from the Drake Passage in spring (Browning et al. 2021). Considering that the dissolved Mn concentrations observed in our study are roughly an order of magnitude higher than those measured in the Southern Ocean where Mn–Fe co-limitation was observed, and Mn* values were all above 1.5, it is unlikely that Mn limitation would have been an important driver shaping phytoplankton communities here. Both dissolved Fe and dissolved Mn have similar coastal sources with dust (Duce and Tindale 1991; Guieu et al. 1994; Baker et al. 2016) and reducing sediments (Homoky et al. 2016) being especially important, thus the dissolved Mn may be acting as a tracer of past dissolved Fe (and other dissolved metal) inputs. In other words, the fact that dissolved Mn concentrations are similar in both eddies could be indicative of eddy II initially having had dissolved Fe concentrations of the same magnitude of those observed in eddy I when it originated near Cape Mendocino. Viewed in this light, the increase in the correlation coefficient when dissolved Mn is included as a factor could reflect that the biological community is influenced not only by being in an eddy (salinity, SST) and dissolved Fe

limitation status (dissolved Fe), but by the initial dissolved metal inputs when the parcel was near coastal sources (dissolved Mn). However, with only correlations to support this hypothesis, it is merely speculative.

Rhizosolenia dominance of eddy II

We note that *Rhizosolenia*, a genus of diatoms with high Si requirements known to have strategies that help overcome N limitation (Villareal et al. 1996), was the most abundant diatom genus recovered from the eddy II stations. One OTU_{99} (*Rhizosolenia* sp. 6) accounted for 40% or more of the diatom community at all seven eddy II stations, with three of these stations having communities dominated by more than 70% *Rhizosolenia* sp. 6. The two eddy II stations with marginally reduced *Rhizosolenia* sp. 6 relative abundance, 4 and 8, also had the lowest observed Si : N ratios in eddy II, indicating a potential shift towards Si limitation. Interestingly, Sta. 20 in eddy I exhibited the highest Si concentration across the entire transect, the highest Si:N ratio within eddy I (> 1), and the highest relative abundance of *Rhizosolenia* sp. 6 outside of eddy II. We acknowledge that 18S copy number per cell is known to vary in response to biovolume in diatoms (Godhe et al. 2008) and *Rhizosolenia* spp. tend to have high biovolumes (Olenina et al. 2006). Thus, in terms of cell counts, *Rhizosolenia* may not have been numerically dominant in eddy II, but it nonetheless dominated the diatom biomass in these samples.

Some species within the *Rhizosolenia* genus can form mats that migrate vertically to access deep N pools using a buoyancy mechanism regulated by cellular carbohydrate ballasting (Villareal et al. 1996). Isotopic and optical methods have shown that *Rhizosolenia* can access N from as deep as 305 m (Pilskaln et al. 2005). Vertical migration of *Rhizosolenia* mats is asynchronous, non-diurnal migration (Villareal et al. 1996). In contrast to upwelling events, which bring both C and N to the surface, when *Rhizosolenia* mats migrate vertically, they access new N below the euphotic zone and then return to the surface to carry out photosynthesis, removing C from surface waters more efficiently than nonvertically migrating phytoplankton (Wilson and Qiu 2008). Thus, a dominant, recurring presence of *Rhizosolenia* mats in California Current System eddies could impact regional C cycling and export estimates. Mat accumulation at the surface occurs for several days at a time (Richardson et al. 1998), especially during low-wind periods (Villareal et al. 1996). Eight species of *Rhizosolenia* have been identified in mats in the NE Pacific, including *R. castracanei*, *R. debyana*, *R. acuminata*, *R. formosa*, *R. ostenfeldii*, *R. decipiens*, *R. fallax*, and *R. shrubsolei* (Carpenter et al. 1977; Villareal and Carpenter 1989). Unfortunately, the majority of the *Rhizosolenia* species previously identified as mat formers are not yet represented in NCBI 18S sequences, including *R. castracanei*, *R. debyana*, *R. acuminata*, *R. ostenfeldii*, and *R. decipiens*. The absence of these 18S sequences could explain the low match percentages (~ 90%) of our *Rhizosolenia* 18S sequences to the *R. shubsholei* 18S sequence (Tables S1 and S2). One species of *Rhizosolenia*, *R. clevei*, which is also not in the sequence library, is known to host the cyanobacterium *Richelia intracellularis* as an endosymbiont in a diatom-diazotroph assemblage (DDA) (Villareal and Carpenter 1989) where *R. intracellularis* fixes dinitrogen (N_2) into a bioavailable form of nitrogen transferring as much as 97.3% of the total fixed nitrogen to its diatom host (Foster et al. 2011). While most of the *Rhizosolenia* sequences from our study cannot be unequivocally confirmed as either a vertically migrating species or the DDA species, several lines of evidence suggest that the sequences observed belong to mat-forming, vertically migrating *Rhizosolenia* species. The top BLASTN hits were that of a previously identified mat-former and vertical migrator, *R. shrubsolei*. The presence of two distinct OTU_{99} of *Rhizosolenia* with elevated relative abundances in eddy II, suggests the possibility that they formed a multi-species mat, as has been found in previous studies (Villareal and Carpenter 1989). In addition, the low wind speed conditions (8–12 m s^{-1}) in eddy II (Fig. S3) would be suitable, though near the upper limit, for *Rhizosolenia* mats to remain intact (Villareal and Carpenter 1989; Villareal et al. 1996). Finally, the process of N_2 fixation for diazotrophs is energetically expensive and dependent on sufficient Fe bioavailability (Falkowski et al. 1998). Because eddy II surface waters had very low dissolved Fe concentrations, N_2 fixation may have been Fe-limited at the time of sampling.

Community succession framework, study limitations, and remaining questions

Given the unique situation in that we were able to sample two eddies that formed in roughly the same region 2 months apart, one way to interpret our dataset is to view it as a study of diatom succession in California Current System eddies. Viewed as such, our data suggest that once an eddy evolves over time into a later-stage, offshore eddy, the phytoplankton communities are substantially distinct from the originally trapped coastal communities because of ecological succession driven by the aging eddy's shifting physicochemical properties. We have provided a schematic to illustrate this diatom community progression showing that high-nutrient, high-diversity coastal waters are initially dominated by coastal diatoms known to have high macro- and micro-nutrient requirements and that as surface nutrient concentrations within the eddy are drawn down over time, species equipped with low-nutrient adaptations can become dominant, altering diatom community diversity (Fig. 7). We do need to acknowledge potential limitations of interpreting our study using this framework. Eddy I formed 1 month prior to sampling around mid-June while eddy II formed 3 months prior to sampling around mid-April. Phytoplankton communities in the California Current System region have been shown to undergo

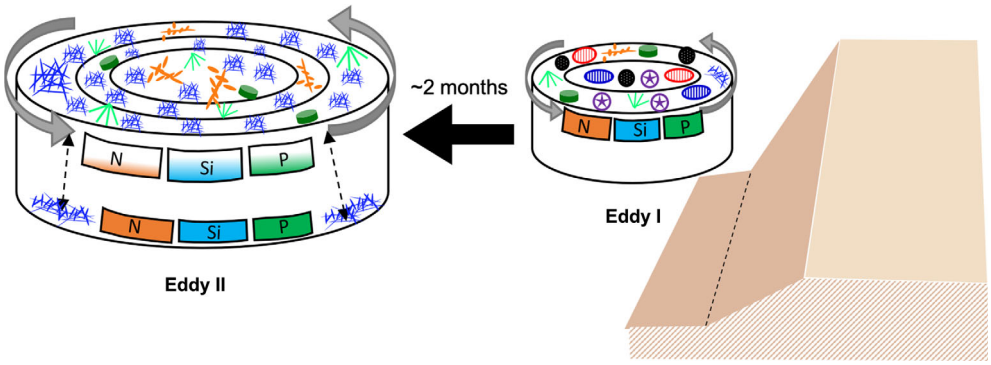

Fig. 7. Schematic representation of diatom ecological succession during eddy aging and propagation offshore. Eddy I is the cylindrical feature spinning counterclockwise on the right side; the eastern boundary of this eddy is located above the continental shelf, shown here as the beige boxes. On the surface of eddy I, there is a diverse community of diatoms. The three boxes on the front of eddy I represent the high-nutrient coastal environment with replete levels of nitrate, silicate, and phosphate. Eddy II is the cylindrical shape on the left side, also spinning counterclockwise, and represents a time-lapse of 2 months after eddy I. On the surface of eddy II, there is a low-diversity community of diatoms dominated by *Rhizosolenia* (blue mats) in a low-nutrient environment. Mats access nutrient-replete waters below the euphotic zone by vertically migrating, as shown by the arrows.

consistent seasonal shifts in composition (Du and Peterson 2013; Peterson et al. 2017). That said, a study in the upwelling region near Bodega Bay found nearly identical coastal diatom communities, including elevated relative abundances of *Chaetoceros* and *Rhizosolenia*, in yearly intervals in the mid-May to late-June timeframe despite high turbulence and mixing (Lassiter et al. 2006). Given that eddy formation was separated by only 2 months, it seems unlikely that differences in the timing of eddy formation led to the marked differences in diatom community observed in eddies I and II. However, as there were no samples obtained at the time of either eddy formation, the degree of influence of seasonality in ecological succession in aging eddies will remain unknown. In addition, while diatoms are known to dominate in waters with Si:N > 1 (Sommer 1994, 1998), some of our sampling stations did have Si:N < 1, which could suggest the importance of other phytoplankton. Indeed, it is well-established that upwelling influenced phytoplankton communities in the California Current System do often progress to be dominated by nondiatom groups (Wilkerson et al. 2006; Krause et al. 2020). As we only examined diatom communities, we are unable to make any conclusions related to overall phytoplankton succession within eddies in the California Current System.

To enable us to generate a high-resolution, synoptic view of the diatom community composition across two cyclonic eddies of differing age, our study sampled only from the surface. That said, we acknowledge that collecting depth-resolved data could have helped to clarify the vertical physicochemical structure of the water column throughout the transect. To provide a comprehensive view of biological activity and export in California Current System eddies, capable of resolving evidence of vertical migration of *Rhizosolenia* (a non-trivial task), future studies should incorporate long-term, Lagrangian sampling of cyclonic eddies that include measurements of C export associated with mats. In the case of this study, we are limited in our ability to assess export or the potential for *Rhizosolenia* migration as we did not make any measurements of biogenic silica or particulate organic C or nitrogen and did not do Lagrangian analyses. While we did not make any associated measurements that could quantify this in our study, diatom community diversity is known to influence C export (Treguer et al. 2018 and references therein).

Conclusions

This study provides valuable insights into the impact of mesoscale cyclonic eddy dynamics on diatom communities in the California Current System, where the high nonlinearity of the eddies severely limits their ability to mix with or incorporate surrounding waters. Our results suggest that both the physicochemical and diatom community structure within cyclonic eddies evolve during propagation offshore. The combined effect of transport by, and ecological succession within the eddies is likely a key factor in mediating C cycling and export across the wider California Current System region. Incorporation of ecological succession in studies of biophysical interactions of eddies can help to clarify C cycling and C export estimates as well as the estimate of total N transported by eddies across the California Current System. In addition, our results suggest that while there may initially be elevated biological activity within a cyclonic eddy, it will eventually plateau following the depletion of nutrients by coastal communities. Finally, the estimates for C cycling and export in the region may need to be revisited to account for vertically-migrating *Rhizosolenia* mats.

Data availability statement

The data repository for this manuscript is hosted at the Biological & Chemical Oceanography Data Management Office (https://www.bco-dmo.org/dataset/876590). Sequencing data

can be found in the NCBI Sequence Read Archive (Bioproject accession # PRJNA743307): https://www.ncbi.nlm.nih.gov/bioproject/PRJNA743307. Access to the complete dataset from the underway system for the MV1405 cruise is available via the Rolling Deck Repository: rvdata.us/search/cruise/MV1405.

References

Altschul, S. F., W. Gish, W. Miller, E. W. Myers, and D. J. Lipman. 1990. Basic local alignment search tool. J. Mol. Bio. **215**: 403–410. doi:10.1016/S0022-2836(05)80360-2

Anderson, M. J., and T. J. Willis. 2003. Canonical analysis of principal coordinates: a useful method of constrained ordination for ecology. Ecology **84**: 511–525. doi:10.1890/0012-9658(2003)084[0511:CAOPCA]2.0.CO;2

Baker, A., and others. 2016. Trace element and isotope deposition across the air–sea interface: progress and research needs. Philos. Trans. A Math. Phys. Eng. Sci. **374**: 20160190. doi:10.1098/rsta.2016.0190

Batteen, M. L., N. J. Cipriano, and J. T. Monroe. 2003. A large-scale seasonal modeling study of the California Current System. J. Oceanogr. **59**: 545–562. doi:10.1023/B:JOCE.0000009585.24051.cc

Behrenfeld, M. J., and E. Boss. 2006. Beam attenuation and chlorophyll concentration as alternative optical indices of phytoplankton biomass. J. Mar. Res. **64**: 431–451. doi:10.1357/002224006778189563

Benoiston, A. S., F. M. Ibarbalz, L. Bittner, L. Guidi, O. Jahn, S. Dutkiewicz, and C. Bowler. 2017. The evolution of diatoms and their biogeochemical functions. Philos. Trans. R. Soc. Lond. B Biol. Sci. **372**: 20160397. doi:10.1098/rstb.2016.0397

Bibby, T. S., M. Y. Gorbunov, K. W. Wyman, and P. G. Falkowski. 2008. Photosynthetic community responses to upwelling in mesoscale eddies in the subtropical North Atlantic and Pacific Oceans. Deep-Sea Res. II **55**: 1310–1320. doi:10.1016/j.dsr2.2008.01.014

Biller, D. V., and K. W. Bruland. 2012. Analysis of Mn, Fe, Co, Ni, Cu, Zn, Cd, and Pb in seawater using the Nobias-chelate PA1 resin and magnetic sector inductively coupled plasma mass spectrometry (ICP-MS). Mar. Chem. **130-131**: 12–20. doi:10.1016/j.marchem.2011.12.001

Biller, D. V., and K. W. Bruland. 2014. The central California Current transition zone: A broad region exhibiting evidence for iron limitation. Prog. Oceanogr. **120**: 370–382. doi:10.1016/j.pocean.2013.11.002

Bray, J. R., and J. T. Curtis. 1957. An ordination of the upland forest communities of southern Wisconsin. Ecol. Monogr. **27**: 325–349. doi:10.2307/1942268

Brown, S. L., M. R. Landry, K. E. Selph, E. J. Yang, Y. M. Rii, and R. Bidigare. 2008. Diatoms in the desert: Plankton community response to a mesoscale eddy in the subtropical North Pacific. Deep-Sea Res. II **55**: 1321–1333. doi:10.1016/j.dsr2.2008.02.012

Browning, T. J., E. P. Achterberg, A. Engel, and E. Mawji. 2021. Manganese co-limitation of phytoplankton growth and major nutrient drawdown in the Southern Ocean. Nat. Commun. **12**: 884. doi:10.1038/s41467-021-21122-6

Bruland, K. W., E. L. Rue, and G. J. Smith. 2001. Iron and macronutrients in California coastal upwelling regimes: Implications for diatom blooms. Limnol. Oceanogr. **46**: 1661–1674. doi:10.4319/lo.2001.46.7.1661

Bruland, K. W., E. L. Rue, G. J. Smith, and G. R. DiTullio. 2005. Iron, macronutrients and diatom blooms in the Peru upwelling regime: brown and blue waters of Peru. Mar. Chem. **93**: 81–103. doi:10.1016/j.marchem.2004.06.011

Brzezinski, M. A., and others. 2002. A switch from $Si(OH)_4$ to NO_3^- depletion in the glacial Southern Ocean. Geophys. Res. Lett. **29**: 5-1–5-4. doi:10.1029/2001gl014349

Callahan, B. J., P. J. McMurdie, M. J. Rosen, A. W. Han, A. J. A. Johnson, and S. P. Holmes. 2016. DADA2: High-resolution sample inference from Illumina amplicon data. Nat. Methods **13**: 581–583. doi:10.1038/nmeth.3869

Capone, D. G., and D. A. Hutchins. 2013. Microbial biogeochemistry of coastal upwelling regimes in a changing ocean. Nat. Geosci. **6**: 711–717. doi:10.1038/ngeo1916

Caron, D. A., and S. K. Hu. 2019. Are we overestimating protistan diversity in nature? Trends Microbiol. **27**: 197–205. doi:10.1016/j.tim.2018.10.009

Carpenter, E. J., G. R. Harbison, L. P. Madin, N. R. Swanberg, D. C. Biggs, E. M. Hulbert, V. L. McAlister, and J. J. McCarthy. 1977. *Rhizosolenia* mats. Limnol. Oceanogr. **22**: 739–741. doi:10.4319/lo.1977.22.4.0739

Chappell, P. D., E. V. Armbrust, K. A. Barbeau, R. M. Bundy, J. Vedamati, and B. D. Jenkins. 2019. Patterns of diatom diversity correlate with dissolved trace metal concentrations and longitudinal position in the northeast Pacific coastal-offshore transition zone. Mar. Ecol. Prog. Ser. **609**: 69–86. doi:10.3354/meps12810

Chenillat, F., P. J. S. Franks, X. Capet, P. Rivière, N. Grima, B. Blanke, and V. Combes. 2018. Eddy properties in the Southern California Current System. Ocean Dyn. **68**: 761–777. doi:10.1007/s10236-018-1158-4

Chenillat, F., P. J. Franks, and V. Combes. 2016. Biogeochemical properties of eddies in the California Current System. Geophys. Res. Lett. **43**: 5812–5820. doi:10.1002/2016GL068945

Clarke, K. R., and M. Ainsworth. 1993. A method of linking multivariate community structure to environmental variables. Mar. Ecol. Prog. Ser. **92**: 205–219. doi:10.3354/meps092205

Clayton, S., S. Dutkiewicz, O. Jahn, and M. J. Follows. 2013. Dispersal, eddies, and the diversity of marine phytoplankton. Limnol. Oceanogr.: Fluids Environ. **3**: 182–197. doi:10.1215/21573689-2373515

Closset, I., H. M. McNair, M. A. Brzezinski, J. W. Krause, K. Thamatrakoln, and J. L. Jones. 2021. Diatom response to alterations in upwelling and nutrient dynamics associated with climate forcing in the California Current System. Limnol. Oceanogr. **66**: 1578–1593. doi:10.1002/lno.11705

Combes, V., F. Chenillat, E. Di Lorenzo, P. Rivière, M. Ohman, and S. Bograd. 2013. Cross-shore transport variability in the California Current: Ekman upwelling vs. eddy dynamics. Prog. Oceanogr. **109**: 78–89. doi:10.1016/j.pocean.2012.10.001

Cushing, D. H. 1971. Upwelling and the production of fish. Adv. Mar. Biol. **9**: 255–334. doi:10.1016/S0065-2881(08)60344-2

Du, X., and W. T. Peterson. 2013. Seasonal cycle of phytoplankton community composition in the coastal upwelling system off central Oregon in 2009. Estuaries Coasts **37**: 299–311. doi:10.1007/s12237-013-9679-z

Duce, R. A., and N. W. Tindale. 1991. Atmospheric transport of iron and its deposition in the ocean. Limnol. Oceanogr. **36**: 1715–1726. doi:10.4319/lo.1991.36.8.1715

Dugdale, R. C., F. P. Wilkerson, and H. J. Minas. 1995. The role of a silicate pump in driving new production. Deep-Sea Res. I **42**: 697–719. doi:10.1016/0967-0637(95)00015-X

Dunn, O. J. 1964. Multiple comparisons using rank sums. Technometrics **6**: 241–252. doi:10.2307/1266041

Engel, A., S. Goldthwait, U. Passow, and A. Alldredge. 2002. Temporal decoupling of carbon and nitrogen dynamics in a mesocosm diatom bloom. Limnol. Oceanogr. **47**: 753–761. doi:10.4319/lo.2002.47.3.0753

Falkowski, P. G., R. T. Barber, and V. V. Smetacek. 1998. Biogeochemical controls and feedbacks on ocean primary production. Science **281**: 200–207. doi:10.1126/science.281.5374.200

Flierl, G., and D. J. McGillicuddy. 2002. Mesoscale and submesoscale physical-biological interactions, p. 113–185. *In* A. R. Robinson, M. J.J., and B. Rothschild [eds.], The sea. John Wiley & Sons.

Foster, R. A., M. M. Kuypers, T. Vagner, R. W. Paerl, N. Musat, and J. P. Zehr. 2011. Nitrogen fixation and transfer in open ocean diatom-cyanobacterial symbioses. ISME J. **5**: 1484–1493. doi:10.1038/ismej.2011.26

Gloor, G. B., J. M. Macklaim, V. Pawlowsky-Glahn, and J. J. Egozcue. 2017. Microbiome datasets are compositional: and this is not optional. Front. Microbiol. **8**: 2224. doi:10.3389/fmicb.2017.02224

Godhe, A., M. E. Asplund, K. Harnstrom, V. Saravanan, A. Tyagi, and I. Karunasagar. 2008. Quantification of diatom and dinoflagellate biomasses in coastal marine seawater samples by real-time PCR. Appl. Environ. Microbiol. **74**: 7174–7182. doi:10.1128/AEM.01298-08

Guieu, C., R. Duce, and R. Arimoto. 1994. Dissolved input of manganese to the ocean: Aerosol source. J. Geophys. Res.: Atmos. **99**: 18789–18800. doi:10.1029/94JD01120

Harris, C. R., and others. 2020. Array programming with NumPy. Nature **585**: 357–362. doi:10.1038/s41586-020-2649-2

Homoky, W. B., and others. 2016. Quantifying trace element and isotope fluxes at the ocean–sediment boundary: A review. Philos. Trans. A Math. Phys. Eng. Sci. **374**: 20160246. doi:10.1098/rsta.2016.0246

Hood, R. R., M. R. Abbott, A. Huyer, and P. M. Kosro. 1990. Surface patterns in temperature, flow, phytoplankton biomass, and species composition in the coastal transition zone off northern California. J. Geophys. Res.: Oceans **95**: 18081–18094. doi:10.1029/JC095iC10p18081

Hoover, S. M., and A. M. Tréhu. 2017. Uplift, emergence, and subsidence of the Gorda escarpment basement ridge offshore Cape Mendocino, CA. Geochem. Geophys. Geosyst. **18**: 4503–4521. doi:10.1002/2017GC007128

Hutchins, D. A., and K. W. Bruland. 1998. Iron-limited diatom growth and Si:N uptake ratios in a coastal upwelling regime. Nature **393**: 561–564. doi:10.1038/31203

Hutchins, D. A., G. R. DiTullio, Y. Zhang, and K. W. Bruland. 1998. An iron limitation mosaic in the California upwelling regime. Limnol. Oceanogr. **43**: 1037–1054. doi:10.4319/lo.1998.43.6.1037

Iles, A. C., T. C. Gouhier, B. A. Menge, J. S. Stewart, A. J. Haupt, and M. C. Lynch. 2012. Climate-driven trends and ecological implications of event-scale upwelling in the California Current System. Glob. Change Biol. **18**: 783–796. doi:10.1111/j.1365-2486.2011.02567.x

Jost, L. 2006. Entropy and diversity. Oikos **113**: 363–375. doi:10.1111/j.2006.0030-1299.14714.x

Kiefer, D. A. 1973. Chlorophyll *a* fluorescence in marine centric diatoms: Responses of chloroplasts to light and nutrient stress. Mar. Biol. **23**: 39–46. doi:10.1007/BF00394110

Kooistra, W. H., R. Gersonde, L. K. Medlin, and D. G. Mann. 2007. The origin and evolution of the diatoms: Their adaptation to a planktonic existence, p. 207–249. *In* P. G. Falkowski and A. H. Knoll [eds.], Evolution of primary producers in the sea. Elsevier. doi:10.1016/B978-012370518-1/50012-6

Krause, J. W., M. A. Brzezinski, J. L. Largier, H. M. McNair, M. Maniscalco, K. D. Bidle, A. E. Allen, and K. Thamatrakoln. 2020. The interaction of physical and biological factors drives phytoplankton spatial distribution in the northern California Current. Limnol. Oceanogr. **65**: 1974–1989. doi:10.1002/lno.11431

Kruskal, W. H., and W. A. Wallis. 1952. Use of ranks in one-criterion variance analysis. J. Am. Stat. Assoc. **47**: 583–621. doi:10.2307/2280779

Kurian, J., F. Colas, X. Capet, J. C. McWilliams, and D. B. Chelton. 2011. Eddy properties in the California current system. J. Geophys. Res.: Oceans **116**: C08027. doi:10.1029/2010JC006895

Lampe, R. H., and others. 2018. Divergent gene expression among phytoplankton taxa in response to upwelling. Environ. Microbiol. **20**: 3069–3082. doi:10.1111/1462-2920.14361

Lassiter, A. M., F. P. Wilkerson, R. C. Dugdale, and V. E. Hogue. 2006. Phytoplankton assemblages in the CoOP-

WEST coastal upwelling area. Deep-Sea Res. II **53**: 3063–3077. doi:10.1016/j.dsr2.2006.07.013

Levasseur, M. E., and J.-C. Therriault. 1987. Phytoplankton biomass and nutrient dynamics in a tidally induced upwelling: the role of the NO_3:SiO_4 ratio. Mar. Ecol. Prog. Ser. **39**: 87–97.

Lewitus, E., L. Bittner, S. Malviya, C. Bowler, and H. Morlon. 2018. Clade-specific diversification dynamics of marine diatoms since the Jurassic. Nat. Ecol. Evol. **2**: 1715–1723. doi:10.1038/s41559-018-0691-3

Li, W., and A. Godzik. 2006. Cd-hit: a fast program for clustering and comparing large sets of protein or nucleotide sequences. Bioinformatics **22**: 1658–1659. doi:10.1093/bioinformatics/btl158

Mantel, N. 1967. The detection of disease clustering and a generalized regression approach. Cancer Res. **27**: 209–220.

Marchetti, A., M. T. Maldonado, E. S. Lane, and P. J. Harrison. 2006. Iron requirements of the pennate diatom *Pseudo-nitzschia*: Comparison of oceanic (high-nitrate, low-chlorophyll waters) and coastal species. Limnol. Oceanogr. **51**: 2092–2101. doi:10.4319/lo.2006.51.5.2092

Martin, J. M., R. M. Gordon, and S. E. Fitzwater. 1990. Iron in Antarctic waters. Nature **345**: 156–158. doi:10.1038/345156a0

McDougall, T. J., and P. M. Barker. 2011. Getting started with TEOS-10 and the Gibbs Seawater (GSW) Oceanographic Toolbox. SCOR/IAPSO WG127.

McGillicuddy, D. J. 2016. Mechanisms of physical-biological-biogeochemical interaction at the oceanic mesoscale. Ann. Rev. Mar. Sci. **8**: 125–159. doi:10.1146/annurev-marine-010814-015606

McMurdie, P. J., and S. Holmes. 2013. phyloseq: An R package for reproducible interactive analysis and graphics of microbiome census data. PLoS One **8**: e61217. doi:10.1371/journal.pone.0061217

McNair, H. M., M. A. Brzezinski, and J. W. Krause. 2018. Diatom populations in an upwelling environment decrease silica content to avoid growth limitation. Environ. Microbiol. **20**: 4184–4193. doi:10.1111/1462-2920.14431

Middag, R., H. J. W. D. Baar, M. B. Klunder, and P. Laan. 2013. Fluxes of dissolved aluminum and manganese to the Weddell Sea and indications for manganese co-limitation. Limnol. Oceanogr. **58**: 287–300. doi:10.4319/lo.2013.58E

Middag, R., H. J. W. de Baar, P. Laan, P. H. Cai, and J. C. van Ooijen. 2011. Dissolved manganese in the Atlantic sector of the Southern Ocean. Deep-Sea Res. II **58**: 2661–2677. doi:10.1016/j.dsr2.2010.10.043

Morel, F. M., A. Milligan, and M. Saito. 2003. Marine bioinorganic chemistry: the role of trace metals in the oceanic cycles of major nutrients, p. 113–143. *In* H. D. Holland and K. K. Turekian [eds.], Treatise on geochemistry. Elsevier. doi:10.1016/B0-08-043751-6/06108-9

Nagai, T., N. Gruber, H. Frenzel, Z. Lachkar, J. C. McWilliams, and G. K. Plattner. 2015. Dominant role of eddies and filaments in the offshore transport of carbon and nutrients in the California Current System. J. Geophys. Res.: Oceans **120**: 5318–5341. doi:10.1002/2015JC010889

Oksanen, J., and others. 2020. vegan: Community ecology package. R package version 2. 2019.

Olenina, I., and others. 2006. Biovolumes and size-classes of phytoplankton in the Baltic Sea. HELCOM Balt.Sea Environ. Proc. No. 106.

Oliver, H., and others. 2021. Diatom hotspots driven by western boundary current instability. Geophys. Res. Lett. **48**: e2020GL091943. doi:10.1029/2020GL091943

Owen, R. W. 1980. Eddies of the California Current System: Physical and ecological characteristics, p. 237–263. *In* D. M. Power [ed.], The California Islands: proceedings of a multidisciplinary symposium. Santa Barbara Museum of Natural History.

Parker, C. E., M. T. Brown, and K. W. Bruland. 2016. Scandium in the open ocean: A comparison with other group 3 trivalent metals. Geophys. Res. Lett. **43**: 2758–2764. doi:10.1002/2016gl067827

Parsons, T. R. 1984. A manual of chemical & biological methods for seawater analysis. Pergamon Press.

Pausch, F., K. Bischof, and S. Trimborn. 2019. Iron and manganese co-limit growth of the Southern Ocean diatom *Chaetoceros debilis*. PLoS One **14**: e0221959. doi:10.1371/journal.pone.0221959

Peterson, W. T., J. L. Fisher, P. T. Strub, X. Du, C. Risien, J. Peterson, and C. T. Shaw. 2017. The pelagic ecosystem in the Northern California Current off Oregon during the 2014–2016 warm anomalies within the context of the past 20 years. J. Geophys. Res.: Oceans **122**: 7267–7290. doi:10.1002/2017JC012952

Pielou, E. C. 1966. The measurement of diversity in different types of biological collections. J. Theor. Biol. **13**: 131–144. doi:10.1016/0022-5193(66)90013-0

Pilskaln, C. H., T. A. Villareal, M. Dennett, C. Darkangelo-Wood, and G. Meadows. 2005. High concentrations of marine snow and diatom algal mats in the North Pacific Subtropical Gyre: Implications for carbon and nitrogen cycles in the oligotrophic ocean. Deep-Sea Res. I **52**: 2315–2332. doi:10.1016/j.dsr.2005.08.004

R Core Team. 2021. R: A language and environment for statistical computing. R Foundation for Statistical Computing.

Raven, J. A., M. C. W. Evans, and R. E. Korb. 1999. The role of trace metals in photosynthetic electron transport in O_2-evolving organisms. Photosynth. Res. **60**: 111–150. doi:10.1023/A:1006282714942

Richardson, T. L., J. J. Cullen, D. E. Kelley, and M. R. Lewis. 1998. Potential contributions of vertically migrating *Rhizosolenia* to nutrient cycling and new production in the open ocean. J. Plankton Res. **20**: 219–241. doi:10.1093/plankt/20.2.219

Round, F. E., R. M. Crawford, and D. G. Mann. 1990. The diatoms. Cambridge Univ. Press.

Shannon, C. E. 1948. A mathematical theory of communication. Bell Syst. Tech. J. **27**: 623–656.

Smetacek, V. 1999. Diatoms and the ocean carbon cycle. Protist **150**: 25–32. doi:10.1016/S1434-4610(99)70006-4

Sommer, U. 1994. Are marine diatoms favoured by high Si:N ratios? Mar. Ecol. Prog. Ser. **115**: 309–315. doi:10.3354/meps115309

Sommer, U. 1998. Silicate and the functional geometry of marine phytoplankton. J. Plankton Res. **20**: 1853–1859. doi:10.1093/plankt/20.9.1853

SSALTO/DUACS. n.d. The altimetric Mesoscale Eddy Trajectories Atlas (META3.1exp DT) produced by SSALTO/DUACS and distributed by AVISO+ (https://aviso.altimetry.fr) with support from CNES, in collaboration with IMEDEA. 10.24400/527896/a01-2021.001

Sumper, M., and E. Brunner. 2006. Learning from diatoms: Nature's tools for the production of nanostructured silica. Adv. Funct. Mater. **16**: 17–26. doi:10.1002/adfm.200500616

Sunda, W. G., and S. A. Huntsman. 1983. Effect of competitive interactions between manganese and copper on cellular manganese and growth in estuarine and oceanic species of the diatom *Thalassiosira*. Limnol. Oceanogr. **28**: 924–934. doi:10.4319/lo.1983.28.5.0924

Sunda, W. G., and S. A. Huntsman. 1996. Antagonisms between cadmium and zinc toxicity and manganese limitation in a coastal diatom. Limnol. Oceanogr. **41**: 373–387. doi:10.4319/lo.1996.41.3.0373

Till, C., J. R. Solomon, N. R. Cohen, R. H. Lampe, A. Marchetti, T. H. Coale, and K. W. Bruland. 2019. The iron limitation mosaic in the California Current System: Factors governing Fe availability in the shelf/near-shelf region. Limnol. Oceanogr. **64**: 109–123. doi:10.1002/lno.11022

Treguer, P., and others. 2018. Influence of diatom diversity on the ocean biological carbon pump. Nat. Geosci. **11**: 27–37. doi:10.1038/s41561-017-0028-x

Venrick, E. 2009. Floral patterns in the California Current: The coastal-offshore boundary zone. J. Mar. Res. **67**: 89–111. doi:10.1357/002224009788597917

Villareal, T. A., and E. J. Carpenter. 1989. Nitrogen fixation, suspension characteristics, and chemical composition of *Rhizosolenia* mats in the central North Pacific gyre. Biol. Oceanogr. **6**: 327–345. doi:10.1080/01965581.1988.10749535

Villareal, T. A., S. Woods, J. K. Moore, and K. CulverRymsza. 1996. Vertical migration of *Rhizosolenia* mats and their significance to NO_3^- fluxes in the central North Pacific gyre. J. Plankton Res. **18**: 1103–1121. doi:10.1093/plankt/18.7.1103

Wilkerson, F. P., A. M. Lassiter, R. C. Dugdale, A. Marchi, and V. E. Hogue. 2006. The phytoplankton bloom response to wind events and upwelled nutrients during the CoOP WEST study. Deep-Sea Res. II **53**: 3023–3048. doi:10.1016/j.dsr2.2006.07.007

Willis, A., and J. Bunge. 2015. Estimating diversity via frequency ratios. Biometrics **71**: 1042–1049. doi:10.1111/biom.12332

Willis, A. D., and B. D. Martin. 2022. Estimating diversity in networked ecological communities. Biostatistics **23**: 207–222. doi:10.1093/biostatistics/kxaa015

Wilson, C., and X. Qiu. 2008. Global distribution of summer chlorophyll blooms in the oligotrophic gyres. Prog. Oceanogr. **78**: 107–134. doi:10.1016/j.pocean.2008.05.002

Acknowledgments

The authors would like to thank the captain and crew of the R/V Melville cruise MV1405, Ken W. Bruland as Chief Scientist, and Geoffrey Smith, Travis Mellett, and Amanda Laverty for assistance with sample collection. SC was supported by a Moore/Sloan Data Science and Washington Research Foundation Innovation in Data Science postdoctoral fellowship. CPT and THC were supported by NSF award OCE-1259776 to KWB. ZMA was supported by an NSF Graduate Research Fellowship. All other work was supported by a VA Space Grant Consortium New Investigator grant and NSF award OCE-1524482 to PDC.

Conflict of Interest

None declared.

Submitted 12 October 2021
Revised 20 May 2022
Accepted 21 August 2022

Associate editor: Bingzhang Chen